Geometrical dependence in photoionization of H_2^+ in high-intensity, high-frequency, ultrashort laser pulses

S. Selstø,[1] J. F. McCann,[2] M. Førre,[1] J. P. Hansen,[1] and L. B. Madsen[3]
[1]*Department of Physics and Technology, University of Bergen, N-5007 Bergen, Norway*
[2]*Department of Applied Mathematics and Theoretical Physics, Queen's University Belfast, Belfast, BT7 1NN, Northern Ireland, United Kingdom*
[3]*Department of Physics and Astronomy, Aarhus University, DK-8000 Aarhus C, Denmark*
(Received 10 January 2006; published 6 March 2006)

The ionization dynamics of H_2^+ exposed to high-intensity, high-frequency, ultrashort laser pulses is investigated with two theoretical approaches. The time-dependent Schrödinger equation is solved by a direct numerical method, and a simple two-center interference-diffraction model is studied. The energy and angular distributions of the photoelectron for various internuclear distances and relative orientations between the internuclear axis of the molecule and the polarization of the field are calculated. The main features of the photoelectron spectrum pattern are described well by the interference-diffraction model, and excellent quantitative agreement between the two methods is found. The effect of quantal vibration on the photoelectron spectrum is also calculated. We find that vibrational average produces some broadening of the main features, but that the patterns remain clearly distinguishable.

DOI: 10.1103/PhysRevA.73.033407 PACS number(s): 33.80.Rv, 33.60.−q, 31.15.Qg

I. INTRODUCTION

The creation of light sources in the X-ray and extreme ultraviolet (euv) regions has seen rapid developments in recent years [1]. This generation of sources offers the possibility of focusing coherent light to a spot size ~10 nm or less, with ultrashort pulse durations 10^{-17} s, and extremely high intensities. This technology provides a tool for microscopic analysis in space, time, and the interaction strength with applications in high-resolution imaging, ultrafast spectroscopy, biomicroscopy, and nanofabrication. The generation of pulses on the attosecond time scale and with photon energies as high as 100 eV have been demonstrated [2,3]. These improvements have paved the way for the possibility of resolving electronic processes in materials. For simple molecular systems, the degree of control means it is now possible to align both diatomic and polyatomic molecules [4], with various possible applications, such as optical control of molecular energy transfer [5].

The coupling between the external field of a laser and a molecule is sensitive to the frequency and intensity of the light, but also to its polarization. Since the molecular symmetry, and hence its polarizability tensor is a critical factor, the alignment and orientation of the molecule is very significant. For example, the field ionization of molecules is exponentially sensitive to the potential barrier and consequently the orientation of the field relative to the molecule [6–9]. Hence, an improved understanding of the molecule-light interaction should include geometrical effects. The nonspherical symmetry of a molecule means the effect of the interaction is far more complex than that for atoms. This is the reason why so far no nonperturbative *ab initio* calculation, including all degrees of freedom, has been performed for any diatomic molecule—including the simplest of all; the hydrogen molecular ion. Only within the last ten years has it been feasible to perform intensive simulations that can be compared with detailed experimental studies of the system. Although H_2^+ has been under intense theoretical investigation [10], calculations tend to be limited to some particular geometry [11] or some reduced electronic dimensionality [12].

Recently, we presented a numerical method for solving the time-dependent Schrödinger equation for H_2^+ in an ultrashort, intense, high-frequency field including all three spatial dimensions of the electron [13]. The main focus was the total ionization probability P_I and its dependence on orientation and internuclear separation. In this paper, we investigate the energy and angular distributions of the photoelectrons at various orientations and internuclear separations. The angular distribution for ionization by high-frequency light is investigated by the time-dependent method for a short (few cycle) pulse and compared with a simple model describing the process as an interference-diffraction effect. For short high-frequency pulses the interaction time is of the order of a few femtoseconds or less. Thus rovibrational relaxation can be neglected. However, the initial state of vibration determines the distribution of the nuclei and can play a role. We will briefly investigate the influence of vibration on the photoelectron spectra.

The paper is organized as follows: In Sec. II, we outline the method used in the *ab initio* calculations including a discussion of the transformation to obtain the energy and angular distributions of the photoelectron. Also in Sec. II, the two-center interference model is developed. Finally we consider the effect of the quantal vibration state. The results are presented and interpreted in Sec. III, and the conclusions are drawn in Sec. IV. Atomic units ($m_e=\hbar=e=1$) are used throughout.

II. THEORY

In Fig. 1 the coordinate notation and system geometry is illustrated. The internuclear vector $\boldsymbol{R}$ is taken to be the polar

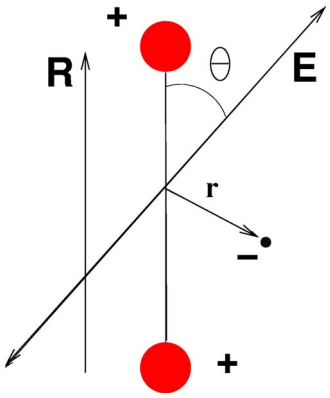

FIG. 1. (Color online) Coordinates (molecular frame); The protons are at a fixed distance R with the molecular axis defining the polar axis (z direction). The xz-plane is chosen so that it contains the polarization vector which defines an angle θ with respect to the z axis. The electron coordinate, with its origin at the midpoint between the nuclei, is denoted by $\mathbf{r}$.

axis in the molecular frame. Suppose the angular frequency of the light is ω, and the duration of the pulse is T. Then a simple representation of the vector potential ($\boldsymbol{A}$) is

$$\boldsymbol{A}(t) = \frac{E_0}{\omega}\sin^2\left(\frac{\pi t}{T}\right)\sin(\omega t + \varphi)\hat{\boldsymbol{u}}_P, \tag{1}$$

where E_0 is the electric field amplitude, the polarization direction $\hat{\mathbf{u}}_P$ is given by the angle θ relative to the internuclear

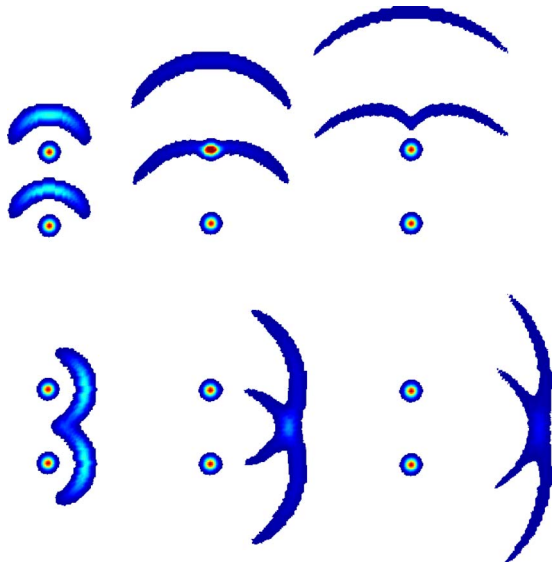

FIG. 2. (Color online) Outgoing waves from each of the scattering centers at three different instants of time (from left to right: t=4, 7, and 10 a.u.). The central energy of the wave packets is 1.1 a.u., and the internuclear separation is 3 a.u. The upper panels correspond to ionization in the direction parallel to the internuclear axis, and the lower ones correspond to perpendicular ionization direction. The scattering centers are shown as circular dots. In the upper case, one of the two outgoing waves is distorted by the upper scattering center, whereas no such interaction takes place in the lower case.

axis, and φ is the phase of the pulse. The calculations presented in this paper are representative of generic strong fields at high frequency. The parameters chosen to illustrate the ionization process are E_0=3 a.u., with central frequency ω =2 a.u. and pulse duration six optical cycles, that is ~450 as. This is far shorter than both the typical vibrational and rotational period of the molecule (15 and 396 fs, respectively). Furthermore, from a classical consideration with an initial internuclear separation 1 a.u., in the extreme case of immediate ionization, the nuclei would move less than 0.2 a.u. during the interaction. Thus we may safely neglect changes in the orientation and the internuclear distance of the molecule during the interaction with the pulse. For a pulse lasting several cycles, the results of the calculations are rather insensitive to the carrier-envelope phase φ. The dipole approximation is well justified for the field applied [14].

A. *Ab Initio* calculations

For fixed internuclear distance, R, and with r_1 and r_2 denoting the distances of the electron from the nuclei, the electronic Hamiltonian in the length gauge is

$$H_L = -\frac{1}{2}\nabla^2 - \frac{1}{r_1} - \frac{1}{r_2} + \frac{1}{2}\boldsymbol{E}(t)\cdot(\boldsymbol{r}_1 + \boldsymbol{r}_2) = -\frac{1}{2}\nabla^2 - \frac{1}{|\boldsymbol{r} - \boldsymbol{R}/2|} - \frac{1}{|\boldsymbol{r} + \boldsymbol{R}/2|} + \boldsymbol{E}(t)\cdot\boldsymbol{r}, \tag{2}$$

or, alternatively, in the Kramers-Henneberger frame (acceleration gauge),

$$H_{KH} = -\frac{1}{2}\nabla^2 - \frac{1}{|\boldsymbol{r} - \boldsymbol{R}/2 + \boldsymbol{\alpha}(t)|} - \frac{1}{|\boldsymbol{r} + \boldsymbol{R}/2 + \boldsymbol{\alpha}(t)|}, \tag{3}$$

with $\boldsymbol{\alpha}(t) \equiv \int_0^t \boldsymbol{A}(t')dt'$.

The wave function is expanded in spherical coordinates as follows:

$$\Psi(\mathbf{r},t) = \sum_{l=0}^{l_{\max}} \sum_{m=-l}^{l} f_{lm}(r,t)Y_{lm}(\Omega), \tag{4}$$

where Y_{lm} are spherical harmonics, and $f_{lm}(r,t)$ are the radial functions that are discretized on a grid of evenly-spaced points. The time-dependent Schrödinger equation is propagated by the split-step method [15,16]. Convergent results were obtained using 2048 radial grid points ranging up to $r_{\max}$=150 a.u. including $l_{\max}$=15 in the expansion Eq. (4). We used this method to construct the ground state Ψ_0 by propagating in "imaginary time" ($t \to \tau = -it$). The eigenenergy can be found from the decay rate of the norms of the wave function, namely,

$$E_0 = -\frac{1}{2\Delta\tau}\ln\left(\frac{\langle\Psi_0(\tau+\Delta\tau)|\Psi_0(\tau+\Delta\tau)\rangle}{\langle\Psi_0(\tau)|\Psi_0(\tau)\rangle}\right). \tag{5}$$

Comparing this value with the exact result provides a good measure of the accuracy of the calculations. For instance, for R=2 a.u., we find that E_0=−1.100 a.u., compared with the exact value—1.103 a.u. [18]. In order to avoid unphysical reflections at the outer boundary of the spherical grid, the wave function is smoothly attenuated at each time step by

multiplying by the factor $g(r)=1-\sin^M[\pi r/(2r_{\max})]$ with $M=20$. The calculations were performed mainly in the length gauge, but also the Kramers-Henneberger formulation of the Hamiltonian was used in order to check for gauge invariance.

We now turn to our method of distinguishing between the bound and the continuum part of the spectrum, and the extraction of the energy spectrum of the photoelectrons. We partition the wave function as the sum of a bound and continuum part, $\Psi=\Psi_{\text{bound}}+\Psi_{\text{out}}$. The separation of the spatial wave function into the two parts is accomplished by allowing the wave packet to propagate some additional time after the pulse is over. At some point t_f after the interaction, the wave packet corresponding to fast photoelectrons will have separated from the bound states, and the bound states are contained within a finite radius $r \leqslant a$. We determine a and t_f by direct inspection of the radial density of the wave function as a function of time. In the present calculations we have allowed the wave packet to propagate for about 13 a.u. after the interaction with the laser pulse has finished ($t_f=T+13$ a.u.). It is important to bear in mind that the distance a must be large enough so that the effect of the Coulomb potential on the kinetic energy of the outgoing electron can be neglected, that is $a \gg 2/k^2$. The continuum function is then transformed to the momentum representation by a Fourier transform

$$\tilde{\Psi}_{\text{out}}(\mathbf{k}) \equiv \mathcal{F}\{\Psi_{\text{out}}(\mathbf{r})\}. \tag{6}$$

From $\tilde{\Psi}_{\text{out}}(\mathbf{k})$ the energy and angular spectra can be obtained. Since we are free to chose the size of the grid, and we can propagate as long as desired, this method should in principle work in any case except for $k \approx 0$. Thus, we expect this method to work best for photon energies well above the ionization potential, as is the case here ($\omega=2$ a.u.).

The Fourier transform of the ionized part is calculated from Eq. (4) as

$$\tilde{\Psi}_{\text{out}}(\mathbf{k}) = \sum_{l=0}^{l_{\max}} \sum_{m=-l}^{l} g_{lm}(k) Y_{lm}(\Omega_k) \tag{7}$$

with

$$g_{lm}(k) = \sqrt{\frac{2}{\pi}}(-i)^l \int_a^\infty j_l(kr) f_{lm}(r,t_f) r^2 dr, \tag{8}$$

where j_l is the spherical Bessel function of the first kind.

The momentum and angular probability distributions can be calculated directly from the momentum space densities as follows:

$$\frac{dP_I}{dk} = \int_{4\pi} k^2 \left|\tilde{\Psi}_{\text{out}}(\boldsymbol{k})\right|^2 d\Omega_k \tag{9}$$

and

$$\frac{dP_I}{d\Omega_k} = \int_0^\infty k^2 \left|\tilde{\Psi}_{\text{out}}(\boldsymbol{k})\right|^2 dk, \tag{10}$$

The energy spectrum can be derived through the relation $dP/dE=(1/k)dP/dk$.

If the photon energy is high and the pulse is long enough, the spectrum will have well-defined peaks associated with absorption of a certain number N of photons. Restricting the integration in Eq. (10) to this k interval, the angular distribution corresponding to absorption of N photons is found.

B. Model

In [13] both the dependence of P_I on θ and R and the angular distribution is a consequence of interference between two isotropic point sources located on the protons. This follows from the fact that it is a good approximation to assume that the initial state, for intermediate and large values of R, is an even-parity superposition of single-center spherical functions, $\Psi_0 \sim \phi_s(r_1)+\phi_s(r_2)$. The agreement between this model and the results from solving the Schrödinger equation is rather good. The model may be further improved by including polarization of the single-center orbitals [17,18] or by including a two-center function reflecting the elliptic symmetry [19].

Applying the same reasoning to the continuum function, we assume the outgoing wave to be of the asymptotic ($t, r \to \infty$) form

$$\psi_{\text{out}} = f_p(\Omega_1)\exp(ikr_1)/r_1 + f_p(\Omega_2)\exp(ikr_2)/r_2. \tag{11}$$

For one-photon absorption, the scattering amplitude f_p corresponds to an atomic p wave rotated along the polarization axis. With $\mathbf{R}$ parallel to the z axis and $\hat{\mathbf{u}}_P$ in the xz plane we have

$$f_p(\Omega_i) \propto \hat{\mathbf{u}}_P \cdot \mathbf{r}_i \propto \cos\theta Y_{10}(\Omega_i) + \sin\theta \frac{1}{\sqrt{2}}[Y_{1-1}(\Omega_i) - Y_{11}(\Omega_i)]. \tag{12}$$

From this, the differential ionization probability is found to be

$$\frac{dP_I}{d\Omega_k} \propto |f_p(\Omega_k)|^2 \cos^2\left(\tfrac{1}{2}\boldsymbol{k}\cdot\boldsymbol{R}\right), \tag{13}$$

where $\Omega_k=\{\theta_k,\phi_k\}$ is the direction of the ionized electron with respect to the polar axis $\mathbf{R}$. We take the value of k to be the one corresponding to the kinetic energy at $r \to \infty$, $k(R)=\sqrt{2[\omega-I_P(R)]}$.

Comparing the predictions of this simple model with our *ab initio* calculations gives broad agreement for the angular distribution. A simple refinement of the initial state allows for the polarization of the orbital, so that the single-center has p wave terms giving angular distributions with additional s and d wave terms. Furthermore, the simple two-center model, while including the interference effect, neglects the scattering effect of the other center; the final state (outgoing spherical waves) can be diffracted by the potential corresponding to the other proton. This effect will be most pronounced when the polarization axis is aligned with the molecular axis. On the other hand, for orthogonal axis and polarization, this refinement should not have much effect. The phenomenon is illustrated in Fig. 2. In effect, all waves passing through the area close to the other scattering center

will be Coulomb shifted. The magnitude of the shift depends on how close to the center it passes, and it is maximal for $\theta_k=0°$ and 180°. In order to capture this effect, the ansatz Eq. (11) should be modified accordingly. The eikonal approximation is one way of realizing this [20,21]

$$\psi'_{\text{out}} = f_p(\Omega_1)\exp\left(i\int_0^{r_1}\sqrt{2[E-V(\mathbf{r}'_1)]}\hat{\mathbf{k}}_1\cdot d\mathbf{r}'_1\right)/r_1 + f_p(\Omega_2)\exp\left(i\int_0^{r_2}\sqrt{2[E-V(\mathbf{r}'_2)]}\hat{\boldsymbol{k}}_2\cdot d\mathbf{r}'_2\right)/r_2, \tag{14}$$

where $E=\omega-I_P$, and the unit vectors $\hat{\boldsymbol{k}}_{1,2}$, parallel to the line segments $d\mathbf{r}'_{1,2}$, point radially outwards from their respective scattering centers. $V(\mathbf{r}_{1,2})$ is the Coulomb potential expressed in coordinates with the respective protons as origins

$$V(\boldsymbol{r}_{1,2}) = -\frac{1}{r_{1,2}} - \frac{1}{|\boldsymbol{r}_{1,2}\pm\boldsymbol{R}|}, \tag{15}$$

where the plus sign corresponds to proton one and the minus sign to proton two. The differential ionization probability is found by letting r become large. It is important to maintain the distinction between r_1 and r_2 in the upper integration limits in Eq. (14), also for large r.

Unfortunately, the singularities in the Coulomb potential cannot be treated adequately within this approximation. The divergences at $\boldsymbol{r}=\pm\boldsymbol{R}/2$ are manifested as discontinuities in the derivative of $dP_I/d\Omega_k$. For this reason we have "softened" the potential; $V\rightarrow V'\equiv -1/\sqrt{r_1^2+s^2}-1/\sqrt{r_2^2+s^2}$. The parameter s is chosen as small as possible while removing the cusps. Outside these regions, the results are not very sensitive to this parameter.

This approach amounts to a differential ionization probability given by

$$\frac{dP_I}{d\Omega_k} \propto |f_p(\Omega_k)|^2 \lim_{r\rightarrow\infty}\left|e^{i\int_0^{r-R/2\cos\theta_k}\sqrt{2[E-V'(\mathbf{r}_1)]}\hat{\boldsymbol{k}}\cdot d\boldsymbol{r}_1} + e^{i\int_0^{r+R/2\cos\theta_k}\sqrt{2[E-V'(\mathbf{r}_2)]}\hat{\boldsymbol{k}}\cdot d\boldsymbol{r}_2}\right|^2. \tag{16}$$

In the limit $s\rightarrow\infty$, Eq. (13), is reobtained.

C. The *R*-averaged spectra

As already pointed out, we do not expect any interference between the dynamics of the direct ionization and the molecular vibration. However, it should be taken into account that the initial state does not have a well defined R value. Neglecting rotation, the initial state is, within the Born-Oppenheimer approximation, the product of an electronic ground state that depends parametrically on R and an internuclear state

$$\Phi_0(R,\boldsymbol{r}) = F(R)\Psi_0(R;\boldsymbol{r}). \tag{17}$$

The internuclear part may be written as a coherent linear combination of vibrational states up to some $\nu_{\max}$,

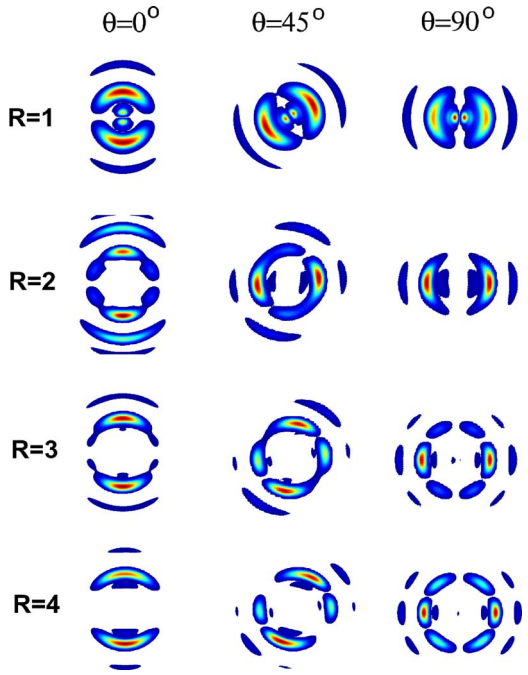

FIG. 3. (Color online) The momentum wave function in the scattering plane, $|\tilde{\Psi}_{\text{out}}(k_x,k_y=0,k_z)|^2$, for various internuclear distances R and relative orientations between the linearly polarized field and the vertical internuclear axis. R increases from top to bottom. To the left, the field and the molecule are parallel ($\theta=0°$) to each other, to the right they are perpendicular to each other ($\theta=90°$), and in the middle we have $\theta=45°$. The internuclear axis points in up/down direction, and the momenta k_x and k_z span from −3 to 3 a.u.

$$F(R) = \sum_{\nu=0}^{\nu_{\max}} c_\nu(t_0)e^{-i\epsilon_\nu t_0}\chi_\nu(R). \tag{18}$$

From this expression, and the linearity of the Schrödinger equation, we assume that a realistic final state may be obtained from our numerical calculations as $\Phi_{\text{final}}(R,\boldsymbol{r}) = F(R)\Psi_R(\boldsymbol{r},t_f)$ where $\Psi_R(\boldsymbol{r},t_f)$ is the solution of the electronic Schrödinger equation with the internuclear distance fixed at R and $t_f>T$. The spectra can then be found in the same manner as before using the "R-averaged" final electronic wave function

$$\bar{\Psi}_{\text{final}}(\boldsymbol{r}) \equiv \frac{1}{R_{\max}-R_{\min}}\int_{R_{\min}}^{R_{\max}} F(R)\Psi_R(\boldsymbol{r},t_f)dR \approx \sum_n w_n F(R_n)\Psi_{R_n}(\boldsymbol{r},t_f), \tag{19}$$

where the weights w_n depend on the set of R_n-s chosen.

The coefficients c_ν in Eq. (18) are determined by the mechanism involved in producing H_2^+. When the molecular ion is made by ionizing H_2-molecules by electron impact, they are usually approximated by the well-known Franck-Condon factors. The amplitudes are also proportional to a dynamic phase factor given by the energy ϵ_ν of the particular vibrational state ν. Consequently, the vibrational state is sub-

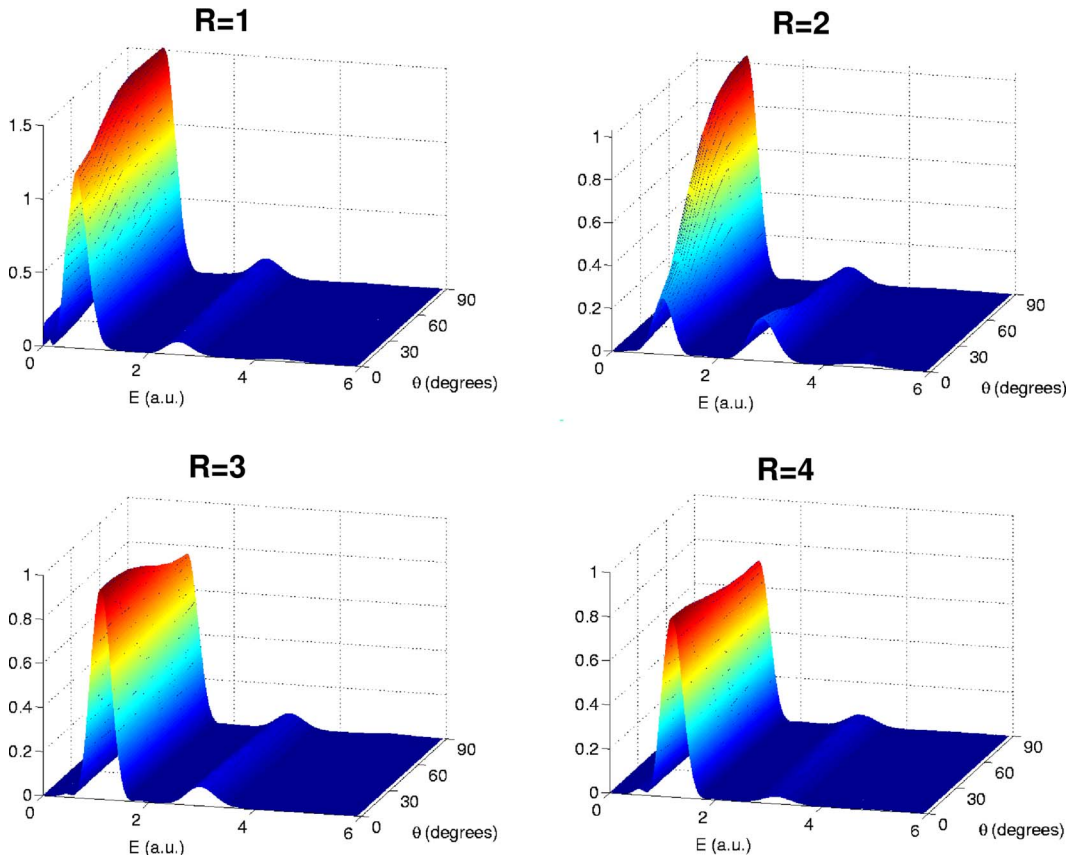

FIG. 4. (Color online) The energy distribution of the photoelectron as a function of kinetic energy of the outgoing electron and the angle θ between the internuclear axis and the field. The distributions correspond to R=1, 2, 3, and 4 a.u. Peaks are seen at $E \approx \omega - I_P$ and $E \approx 2\omega - I_P$ [ω=2 a.u., and $I_P(R)$=1.45, 1.1, 0.91, and 0.80 a.u., respectively]. The one-photon ionization signal dominates the spectrum, and therefore it also governs the dependence of the ionization probability on the relative orientation θ.

ject to a coherent time evolution, which causes a strong variation on the femtosecond time scale. Hence the actual R distribution at the instant the interaction begins, is very sensitive to the time delay t_0 of the pulse [22].

Recently a method based on the strong field approximation was shown to give better agreement with the experiment [23] than the Franck-Condon factors [24]. In this paper it is also suggested that producing a pure ground vibrational state should be quite feasible. Such a state would not give rise to any time-dependent R distribution.

III. RESULTS AND DISCUSSION

In Fig. 3 we display sections of the momentum distribution of the photoelectron in the plane spanned by the field polarization and the internuclear axis, i.e., we consider $|\tilde{\Psi}_{\text{out}}(k_x, k_y=0, k_z)|^2$ as a function of k_x and k_z. The distributions are shown for the internuclear distances R=1, 2, 3, and 4 a.u., and the linear polarization is parallel, perpendicular, and intermediate (θ=45°) relative to $\boldsymbol{R}$. The internuclear axis is oriented in the vertical direction. Both the k_x and the k_z axis extend from −3 a.u. to 3 a.u. in all cases. These figures demonstrate clearly which ionization directions and energies are most probable. The contributions from one- and two-photon ionization are seen as parts of concentric rings in the probability densities. For R=2, θ=0° also probability density stemming from three-photon ionization is observed. For polarization parallel and perpendicular to the internuclear axis, the wave packets have clear maxima in the directions of the field. This is not the case at intermediate polarization directions. This behavior is a signature of interference. At internuclear separation R=1 a.u., the distribution seems to be atomiclike, i.e., a rotation of the field seems to simply amount to a corresponding rotation of the wave packet. But this is in fact not the case; the principal direction of ionization is *not* 45° for the intermediate polarization direction, and, as we will see, the overall ionization probability is strongly θ-dependent. For R=2 a.u., the probability of two-photon ionization is comparable to the probability of one-photon ionization for θ=0°, whereas the one-photon ionization dominates more and more as θ increases towards 90°. For R=3 and 4 a.u., the maxima tend to be more localized, and some local maxima appear in addition to the global ones at perpendicular polarization.

The dependence on the orientation of the field relative to the internuclear axis is shown in Fig. 4. Here we see the energy spectrum dP_I/dE as a function of the polarization angle θ in addition to the energy E. The plots are made for the same internuclear distances as in Fig. 3. All four figures have clear maxima for $E \sim \omega - I_P$, corresponding to the absorption of one photon with energy ω. Peaks corresponding

to two-photon ionization ($E \sim 2\omega - I_P$) can also be seen. The position of the maxima are independent of the polarization angle θ, but the magnitude of the ionization probability exhibit strong θ dependence—in particular for $R=2$ a.u. For $R=1$ and 2 a.u., the ionization probability is highest at the perpendicular polarization, whereas the situation is the contrary for $R=3$ and 4 a.u. These effects can be related to the oscillatory behavior of the total ionization probability $P_I(R)$ as a function of internuclear distance. The oscillations are strong for $\theta=0°$ and absent at $\theta=90°$. This can be understood within the simple model of Eq. (13), as explained in [13]. The probability of ionization by two photons is rather independent of the polarization direction for all internuclear distances at hand. For $R=1$ and 2 a.u., also three-photon ionization is visible on this scale.

Figure 5 shows three-dimensional polar plots of the differential ionization probability, $dP_I/d\Omega_k$, for the same internuclear distances and orientations as in Fig. 3. The radial distance of these surfaces indicates the probability density of ionization in that particular direction. In all figures, the internuclear axis is oriented vertically, and the polarization, indicated by a black line, also lies in the plane of the paper. It should be noted that the figures are not scaled equally. They show, as does Fig. 3, that for parallel and perpendicular orientation, the photoelectron is most likely ionized in the direction of the field. In addition to these global maxima, some local maxima at intermediate angles are observed. These "side lobes" are most clearly visible at $\theta=90°$. They increase in magnitude as R increases, whereas the maxima in the directions of the field become more and more narrow. At intermediate polarization, $\theta=45°$, the polarization direction is *not* the most likely direction of ionization. All of these features clearly indicate that the signal is built up from interferring contributions from the two centers.

The differential ionization probability for one-photon ionization has been calculated and compared with the predictions of the models in Eqs. (13) and (16). The results are shown in Fig. 6. The differential probability is shown in half of the scattering plane as functions of the angle between the ionization direction and the polarization of the field. The full curves show the results obtained from the *ab initio* calculation, whereas the others show the predictions of the models. Due to the rather sharp peaks corresponding to one-photon absorption seen in Fig. 4, the idea of using one well-defined asymptotic k value is justified. We find that our model is able to reproduce the differential one-photon ionization probability quite well. We are therefore confident that the assumption of interferring nonconcentric spherical waves is the adequate one. The approach based on the eikonal approximation in general compensates for the discrepancies between the *ab initio* results and the seemingly naive model, where the anisotropy of the molecular Coulomb potential is not fully accounted for. In general, the two models agree rather well for the polarization angle $\theta=90°$, whereas the deviations can be quite large for $\theta=0°$ and 45°—in particular for $R=2$ and 3 a.u. For small internuclear separations, the system is similar to He^+, for which no diffraction takes place. In the other extreme case, i.e., when R becomes large, a smaller angular range of the outgoing wave passes through the vicinity of the other proton. In both cases, the effect of diffraction is less pronounced than is the case for intermediate internuclear separations, which explains the rather high level of agreement between the two models for $R=1$ and 4 a.u.

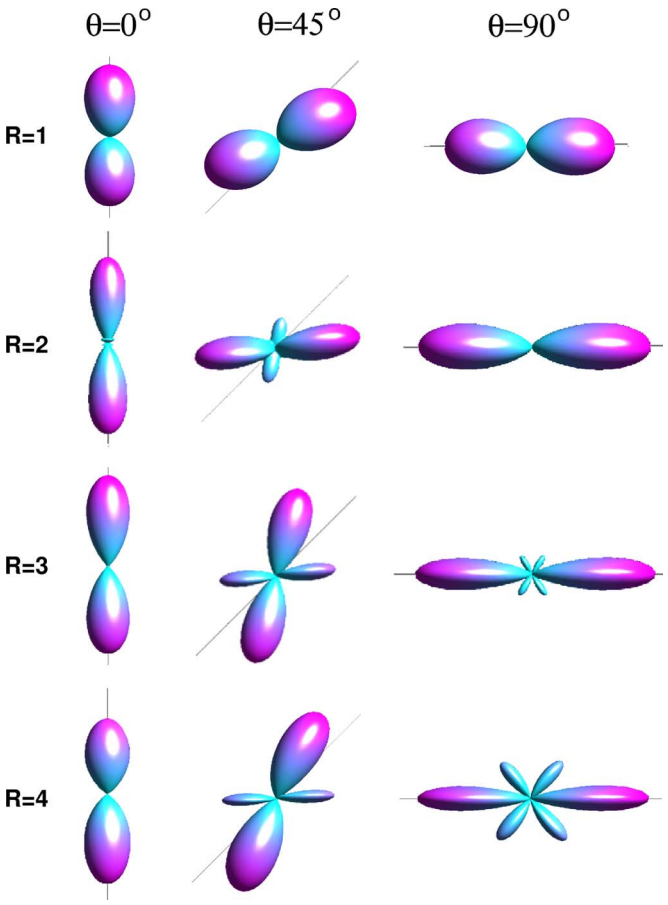

FIG. 5. (Color online) The differential ionization probability at various polarization directions and internuclear separations. The figures are displayed in the same manner as in Fig. 3. The line indicates the direction of the field. The overall scaling varies from figure to figure.

The influence of the initial vibrational state on the final angular distributions of the total differential probability has been investigated for two initial R-distributions, namely the vibrational ground state $\chi_{\nu=0}(R)$, and another state chosen to be a Gaussian centered at $R=2.5$ a.u. with a standard deviation 0.7 a.u. The integration in Eq. (19) has been done by the trapezoidal rule including final electronic wave functions with internuclear separations 1, 1.5, 2, 2.5, 3, and 4 a.u. The results are displayed for both cases along with the corresponding R-distributions in Fig. 7. They should be compared with Fig. 4. We find that taking the vibrational state into account does not wipe out the signatures of the different orientations completely. In the case of the vibrational ground state, all three distributions are clearly distinguishable. With the wider distribution in the lower panels, the $\theta=0°$ and $\theta=45°$ spectra are not that easily distinguished, and we expect that for such a broad distribution of R values and smaller values of θ, the orientation of the molecule cannot be decided as precisely as in the case of a more localized internuclear wave function.

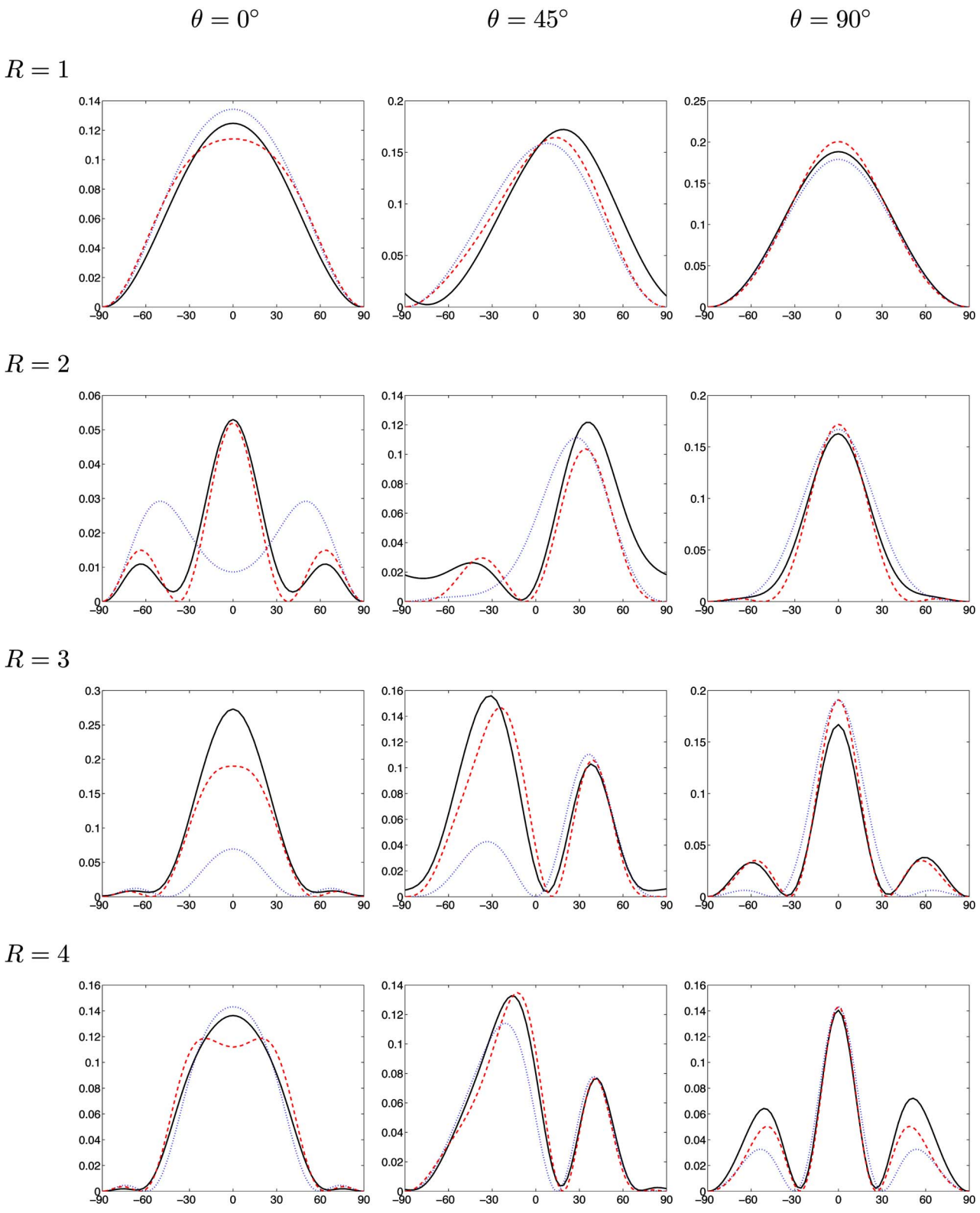

FIG. 6. (Color online) The differential ionization probability for one-photon ionization plotted in the scattering plane. The ordinate is the angle of the outgoing electron relative to the direction of the field. The full curves are the results obtained from solving the Schrödinger equation, the dotted curves are the prediction of the simple interference model, Eq. (13), while the dashed curves are the predictions of the model including diffraction, Eq. (16). The panels are displayed according to geometry in the same manner as Figs. 3 and 5.

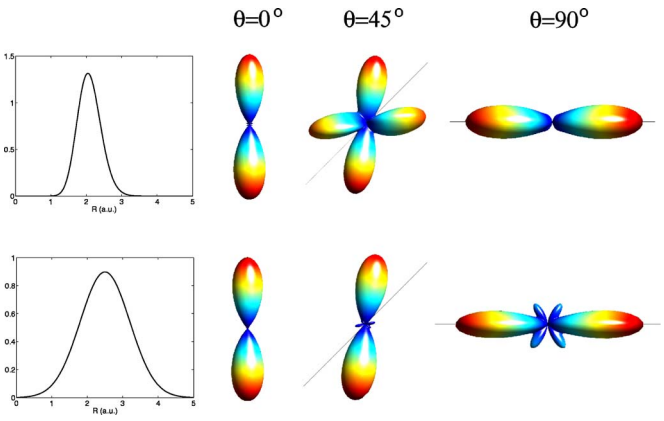

FIG. 7. (Color online) The total differential ionization probability with the initial vibrational state taken into consideration. The upper panels correspond to the vibrational ground state, and the lower ones correspond to a Gaussian distribution centered at $R=2.5$ a.u. with a standard deviation of 0.7 a.u. These vibrational wave functions are shown to the left. As in Fig. 4, the direction of the polarization with respect to the vertical internuclear axis is given by $\theta=0°$, 45°, and 90°, respectively.

IV. CONCLUSIONS

We have investigated the dynamics of high-intensity, high-frequency ionization of H_2^+ by laser fields based on *ab initio* methods as well as simple models. The energy and the angular distributions of the photoelectron have been calculated for various geometries by investigating the ionized part of the wave function. These spectra have been explained as an interference effect between outgoing nonconcentric spherical waves, where the waves are diffracted by the other scattering center.

It was found that the features of the different orientations survive when the vibrational motion is taken into account. This demonstrates that information about the initial molecular orientation is obtainable experimentally from investigating the photoelectron of the molecule after interaction with a laser pulse.

ACKNOWLEDGMENTS

The present research was supported by the Norwegian Research Council through the NANOMAT program and the Nordic Research Board NordForsk. I.B.M. is supported by the Danish Natural Science Research Council (Grant No. 21-03-0163). Finally, we would like to thank Professor Ladislav Kocbach for fruitful discussions and Dr. Alicia Palacios at la Universidad Autónoma de Madrid for her help.

[1] U. Keller, Nature (London) **424**, 831 (2003).
[2] A. Baltuška, Th. Udem, M. Uiberacker, M. Hentschel, E. Goulielmakis, Ch. Gohle, R. Holzwarth, V. S. Yakovlev, A. Scrinzi, T. W. Hänsch, and F. Krausz, Nature (London) **421**, 611 (2003).
[3] R. Kienberger, E. Goulielmakis, M. Uiberacker, A. Baltuska, V. Yakovlev, F. Bammer, A. Scrinzi, Th. Westerwalbesloh, U. Kleineberg, U. Heinzmann, M. Drescher, and F. Krausz, Nature (London) **427**, 817 (2004).
[4] C. Z. Bisgaard, M. D. Poulsen, E. Peronne, S. S. Viftrup, and H. Stapelfeldt, Phys. Rev. Lett. **92**, 173004 (2004).
[5] H. Stapelfeldt and T. Seideman, Rev. Mod. Phys. **75**, 543 (2003).
[6] R. Dörner, H. Bräuning, O. Jagutzki, V. Mergel, M. Achler, R. Moshammer, J. M. Feagin, T. Osipov, A. Bräuning-Demian, L. Spielberger, J. H. McGuire, M. H. Prior, N. Berrah, J. D. Bozek, C. L. Cocke, and H. Schmidt-Böcking, Phys. Rev. Lett. **81**, 5776 (1998).
[7] T. K. Kjeldsen, C. Z. Bisgaard, L. B. Madsen, and H. Stapelfeldt, Phys. Rev. A **68**, 063407 (2003).
[8] T. K. Kjeldsen and L. B. Madsen, Phys. Rev. A **71**, 023411 (2005).
[9] T. K. Kjeldsen, C. Z. Bisgaard, L. B. Madsen, and H. Stapelfeldt, Phys. Rev. A **71**, 013418 (2005).
[10] J. H. Posthumus and J. F. McCann, in *Molecules and Clusters in Intense Laser Fields* (Cambridge Press, Cambridge 2001).
[11] D. Dundas, Phys. Rev. A **65**, 023408 (2002).
[12] B. Rotenberg, R. Taïeb, V. Veniard, and A. Maquet, J. Phys. B **35**, L397 (2002).
[13] S. Selstø, M. Førre, J. P. Hansen, and L. B. Madsen, Phys. Rev. Lett. **95**, 093002 (2005).
[14] M. Førre, S. Selstø, J. P. Hansen, and L. B. Madsen, Phys. Rev. Lett. **95**, 043601 (2005).
[15] M. R. Hermann and J. A. Fleck, Jr., Phys. Rev. A **38**, 6000 (1988).
[16] J. P. Hansen, T. Sørevik, and L. B. Madsen, Phys. Rev. A **68**, 031401(R) (2003).
[17] B. N. Dickinson, J. Chem. Phys. **1**, 317 (1933).
[18] F. Weinhold, J. Chem. Phys. **54**, 530 (1971).
[19] A. Dalgarno and G. Poots, Proc. Phys. Soc., London, Sect. A **67**, 343 (1954).
[20] L. D. Landau and E. M. Lifschitz, in *Quantum Mechanics*, 3rd ed. (Pergamon Press, Oxford, 1977), Section 131.
[21] R. J. Glauber, in *Lectures in Theoretical Physics*, edited by W. E. Brittin and L. G. Dunham (Interscience, New York, 1959), Vol. I, p. 315.
[22] L.-Y. Peng, I. D. Williams, and J. F. McCann, J. Phys. B **38**, 1727 (2005).
[23] X. Urbain, B. Fabre, V. M. Andrianarijaona, J. Jureta, J. H. Posthumus, A. Saenz, E. Baldit, and C. Cornaggia, Phys. Rev. Lett. **92**, 163004 (2004).
[24] T. K. Kjeldsen and L. B. Madsen, Phys. Rev. Lett. **95**, 073004 (2005).